Chemical Geology 558 (2020) 119865

Contents lists available at ScienceDirect

Chemical Geology

journal homepage: www.elsevier.com/locate/chemgeo

Major ion geochemistry in Na-Ca-Mg-K-Cl-SO_4 brines using portable X-ray fluorescence spectrometry

Evan L. Kipnis[a,*,1], Brenda B. Bowen[a,b], Sean J. Hutchings[a], Scott A. Hynek[a,c], Kathleen C. Benison[d]

[a] Department of Geology and Geophysics, University of Utah, Salt Lake City, UT, USA
[b] Global Change and Sustainability Center, University of Utah, Salt Lake City, UT, USA
[c] U.S. Geological Survey, Utah Water Science Center, Salt Lake City, UT, USA
[d] Department of Geology and Geography, West Virginia University, Morgantown, WV, USA

ARTICLE INFO

Editor: Karen Johannesson

Keywords:
Major ion geochemistry
Brine chemistry
X-ray fluorescence
pXRF
Instrument calibration

ABSTRACT

Knowledge of the geochemistry of natural waters contributes to the understanding of Earth systems including crustal evolution, geochemical cycles, precipitation and dissolution of chemical sediments, and limits for extremophilic microorganism, as well as contributing hypotheses about other planets and moons that host chemical sediments. However, the traditional methods for quantification of saline waters presents analytical challenges that can lead to inaccurate or unrelatable results. Here, we demonstrate the accuracy and limits of portable X-ray fluorescence spectrometry (pXRF) for analysis of major ion geochemistry in brines from five continents. Results from a validation sample subset show R^2 values > 0.95 for K^+, Ca^{2+}, SO_4^{2-}, > 0.90 for Mg^{2+}, Cl^-, and 0.85 for Na^+ when compared with sample concentrations reported from external laboratories. Dilution experiments demonstrate that the minimum sensitivity of pXRF photon response by major ion varies from > 1 to > 1000 mg/L. The application of this method for quantifying saline water chemistry presents opportunities for further study of brines on Earth and the exploration of saline systems on other planetary bodies.

Plain language summary: The use of portable X-ray fluorescence spectrometry presents an untapped opportunity for characterization of saline waters. Here, we demonstrate the precision and limits of this proposed method for salt water samples collected from saline lakes and salt playas across the Earth.

1. Introduction

Brine chemistry provides insight into geological processes linked to the evolution of modern and ancient saline environments and the accumulation of solutes. Brines are saline waters with high solute concentrations, specifically with total dissolved solids (TDS) greater than 100,000 mg/L (Carpenter, 1978). The concentration of solutes in brines vary with source of water, regional geology dictating water-rock interactions, climate, and the precipitation of minerals (Hardie and Eugster, 1970; Carpenter, 1978; Warren, 1996). On Earth, brines are present as saline lakes, highly restricted lagoons, some deep marine environments, subsurface basinal groundwater, and hydrothermal waters. Elsewhere in the solar system (e.g. Mars, Europa) there is evidence that liquid waters may be brines (Ojha et al., 2015; Trumbo et al., 2019). The chemistry of brines advance understanding of water-rock interactions, extremophilic ecosystems, planetary crust evolution, discharge of saline waters to lakes and playas, and the hydrological and climatological controls on the precipitation and dissolution of saline minerals.

The chemical analysis of major cations (Na^+, Mg^{2+}, K^+, Ca^{2+}) and anions (SO_4^{2-}, Cl^-, HCO_3^-) in solution is notoriously difficult for brines, especially when accurate concentrations for trace elements are desired. Brines can exhibit extreme ranges for ion concentrations and the speciation of ions will vary (Bowen and Benison, 2009). The preparation of brines for analysis with inductively coupled plasma (ICP) or ion chromatography (IC) methods often require filtration, acidification, temperature control, or sample dilution which can introduce errors (Welch et al., 1996). Studies using these techniques note the incomparable values between analyses, contamination of instrumentation by samples of variable concentrations across multiple orders of magnitude, or charge balance error of major ion chemistry exceeding ± 10%, where reference values for analysis of major ions in fresh waters

* Corresponding author.
E-mail address: evan.kipnis@utah.edu (E.L. Kipnis).
[1] 115 S 1460 E, Rm 383, Salt Lake City, UT, 84112.

https://doi.org/10.1016/j.chemgeo.2020.119865
Received 12 June 2020; Received in revised form 1 September 2020; Accepted 1 September 2020
Available online 03 September 2020
0009-2541/

is considered ± 5% (Bowen and Benison, 2009; Brewer and Spencer, 1969).

Recent advances in portable energy dispersive X-ray fluorescence spectrometers (pXRF) have led to the adoption of pXRF in applications of art authentication, archaeological characterization, as well as rock and sediment elemental quantification (Hunt and Speakman, 2015; Rowe et al., 2012). Work with this instrumentation has helped to identify optimized instrument settings to maximize photon response from rock samples using pXRF (Watts et al., 2018). However, very little work has been done to demonstrate the possibility of pXRF applications for waters, and brines in particular (Melquiades et al., 2011; Pearson et al., 2017; Sánchez-Pomales et al., 2013; Zhou et al., 2018). The objective of this work is to test the potential for pXRF to quantify the major ion chemistry of brines and to identify the lower limits of detection for major ions in waters of decreasing salinity.

2. Materials and methods

2.1. Reference samples

Brines and brackish water samples (n = 64) were collected from wells, lakes, playa surfaces, and canals from locations across five continents (Fig. 1). These sites have been subjects of previous investigations into brine body formation, evaporite sedimentology and microbiology, linkages between crustal evolution and brine chemistry, and more (Benison, 2019; Benison and Karmanocky, 2014; Benison and Bowen, 2015; Bowen et al., 2012; Dickson et al., 2013; Kipnis and Bowen, 2018; Munk et al., 2016; Sirota et al., 2017). Samples were collected over a period from 2007 to 2018 in acid washed (HCl) and deionized (DI) water rinsed bottles, sealed with parafilm, and no acidification, filtration, or temperature control (e.g. freezing, refrigeration) were performed for sample storage.

All samples (n = 64) were analyzed in 2017 or 2018 for reference major ion and trace element chemistry at either American West Analytical Laboratories (AWAL), Activation Laboratories Inc. – Ancaster (ActLabs), or Intrepid Potash – Wendover. At AWAL a subset of samples was analyzed using ICP-MS for cations, ion chromatography (IC) for anions, and titration for alkalinity. At ActLabs a subset of samples was analyzed using ICP-OES for cations, ion chromatography (IC) for anions, and titration for alkalinity. At Intrepid Potash a Panalytical AxiosMax wavelength dispersive XRF (WD-XRF) was used for major ion chemistry. Charge balance calculations were performed on all samples using whatever data was available for the ions H^+, Li^+, Na^+, Mg^{2+}, Al^{3+}, K^+, Ca^{2+}, OH^-, Cl^-, Br^-, HCO_3^- and SO_4^{2-}. Specific conductivity and pH were measured using a calibrated In-Situ Aqua TROLL 500 multiparameter probe at the USGS Utah Water Science Center in 2019. Sample densities and lab-based temperatures were measured using a Mettler Toledo Densito 30 PX digital hydrometer at the University of Utah in 2019 (Table 1).

The brine sample geochemistry was reviewed to characterize the broader sample set (Fig. 1). The TDS values for major ions shows samples ranging from brackish waters to some of the densest natural brines on the planet. Sample pH values range from slightly alkaline to extremely acidic. These data also show that extremely alkaline samples and samples with dominant major anions other than Cl^- are absent from this study. Where charge balances exceeded ± 10% it may have been due to incomplete analyses such that analytes at major ion concentrations were not analyzed. As an example, some brines in the Atacama Desert are high in dissolved NO_3^{2-}, but NO_3^{2-} was not analyzed for reference in any of the samples from this study.

2.2. Instrumentation and sample analysis

In preparation for analysis with a Bruker Tracer III-SD energy dispersive portable XRF (pXRF), samples were heated in an oven to approximately 60 °C to promote dissolution of sub-millimeter to millimeter sized crystals that precipitated in some samples during storage. The pXRF instrument is setup in a stand facing upward with a sample plate and 1.5 μm thick Spectromembrane Etnom® thin-film placed over the top of the instrument (Fig. 2). Heated samples were filtered using #1 qualitative filter paper, approximately 11 μm pore size. A 0.5 mL aliquot was pipetted on to thin-film to suspend the sample above the analyzer aperture and covering the 12 mm^2 area of the X-ray source for this instrument. Each sample was scanned at 15 kV and 25 microamps (μA) using no filter to excite fluorescence from lighter elements (Na−Mn) with He gas applied to the instrument at a flow rate of 200 mL/min to displace atmosphere. Each sample was analyzed for 120 s. For collection of data related to some heavier trace metals (Fe−Sr) a secondary scan was performed on a subset of samples (n = 57) using the yellow filter (Ti, Al) and running the instrument at 40 kV and 10 μA for 120 s without He gas.

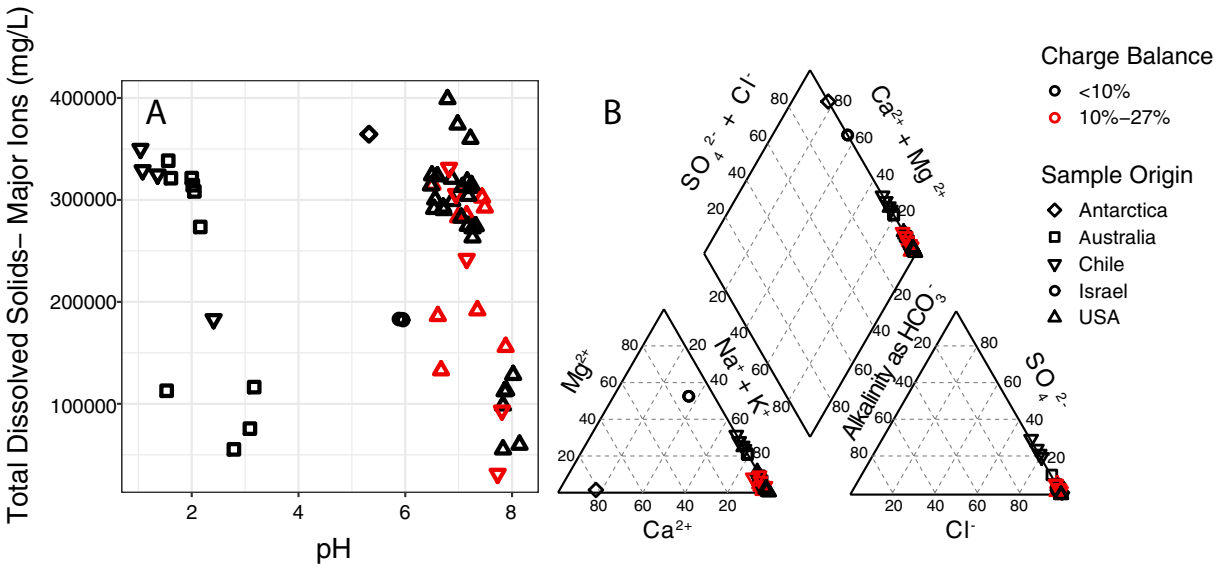

Fig. 1. A) A plot comparing laboratory reference values of Total Dissolved Solids (TDS) from major ion concentrations to pH (n = 60). B) A Piper diagram showing the reference major ion distributions for all samples (n = 64). Sample symbology designates sample origin.

Table 1
A summary of sample chemistry used for this study.

Sample origin	Sample dates	Sample locations	pH	Major ion concentrations (mg/L)							Charge balance
				TDS	Na^+	Mg^{2+}	SO_4^{2-}	Cl^-	K^+	Ca^{2+}	
Antarctica	Mar. 4, 2008	Don Juan Pond	5.32	364,467	13,800	1280	157	234,000	230	115,000	3.4%
Australia	Dec. 31, 2014 – Jan. 4, 2015	Western Australia Acid Saline Lakes	1.53–3.17	55,345–321,422	17,600–108,000	1540–25,000	3360–28,800	32,300–185,000	201–4310	177–570	1.1–6.8%
Chile	Mar. 5, 2007 – Sep. 26, 2012	Salar de Atacama, Salar de Gorbea	1.08–7.81	31,124–349,999	8210–99,200	902–30,600	2370–121,000	17,400–195,000	885–2510	119–2210	2.1–27.0%
Israel	2018	Dead Sea	5.88–5.96	182,216–183,021	14,700–14,800	27,200–27,400	151–165	125,000–126,000	4550–4570	10,200–10,400	0.4–1.3%
USA	May 19, 2011 – Oct. 5, 2018	Bonneville Salt Flats, Great Salt Lake, Clayton Valley, Saline Valley	6.48–8.14	55,067–398,959	18,700–119,845	104–30,500	994–20,600	33,000–244,000	2030–40,300	200–2280	0.1–24.7%

2.3. Inter-Elemental Calibration and Validation

Two calibration models for major ions, one for the measurement of Na^+, Mg^{2+}, and SO_4^{2-} and another for Cl^-, K^+, Ca^{2+} were built using selected pXRF scans and external laboratory reference concentration data ($n = 52$). We assume that observed elemental fluorescence peaks in X-ray spectra were associated with measured major ion concentrations in solution (Na^+, Mg^{2+}, SO_4^{2-}, Cl^-, K^+, Ca^{2+}) rather than other possible dissolved species (e.g. S Kα peak is representative of SO_4^{2-}). To validate these calibration methods, the remaining samples ($n = 12$) were used to produce inter-elemental calibrated concentrations for each major ion from pXRF spectra.

Bruker AXS S1 CalProcesses software was used as previously applied in the analysis of mudrock and sediment cores for the inter-elemental calibration of samples (Rowe et al., 2012). These calibration methods include correction coefficients for spectral slope changes and interferences of overlapping elemental peaks as well as normalization of spectra over a defined energy range. Each prediction included selection of elemental co-predictors for background interference and spectral slope correction factors (Table 2).

2.4. Major ion detection limits for pXRF

A subset of samples ($n = 8$) was incrementally diluted to identify the lower limits of salinity for which this pXRF method shows sensitivity in photon response. Each sample was diluted by factors of approximately 10, 100, 200, 400, 600, 800, and 1000 using 16 MΩ resistivity DI water and reference concentrations were gravimetrically calculated for major ions in diluted samples. Spectra from pXRF of diluted samples were converted to photon counts for each element using the Bayesian deconvolution method in Bruker AXS ARTAX software. With this methodology the user visually identifies the presence of characteristic fluorescence peaks in X-ray spectra and a curve fit deconvolution method outputs interpreted net photon counts from the spectra.

Limits of sensitivity for each major ion were determined using inflection points output from segmented linear regression models comparing photon counts to calculated concentrations of diluted samples for each ion from the R language package 'segmented' (Muggeo, 2017, 2016, 2008, 2003). In these segmented linear regression models a linear model and the number of breakpoints (Ψ) are specified inputs. For the segmented linear regression models used to interpret sensitivity, Ψ values for the prediction of Na^+, Mg^{2+}, SO_4^{2-}, Cl^-, K^+, and Ca^{2+} breakpoints were respectively 2, 2, 1, 1, 1, 2. These were determined by using the fewest number of breakpoints, the ability of a model to reach convergence, and the fit of the segmented linear regression models to the observed data set.

3. Results and discussion

3.1. Brine scans and inter-elemental calibration

Chemical measurements of materials with pXRF involves calibration to the X-ray spectra for a specific material where peaks in the spectra show known characteristic fluorescence of specific elements. The energy of any photon emitted from an atom's electron shell (e.g. K, L, M) during characteristic fluorescence equates to the energy difference between the electron in a higher energy state in a further out electron shell and the lower energy shell an electron moves to. The movement of an electron at higher energy states to a lower energy state is characterized by its movement across one (α) or two (β) electron shell(s), specific to each individual element. Energy from an X-ray source acts to displace electrons from the electron shells of a sample material. The energy of each photon either reflected from the surface of a sample or from the characteristic fluorescence of the atoms in a sample are measured by a detector. The intensity of a fluorescence peak in X-ray

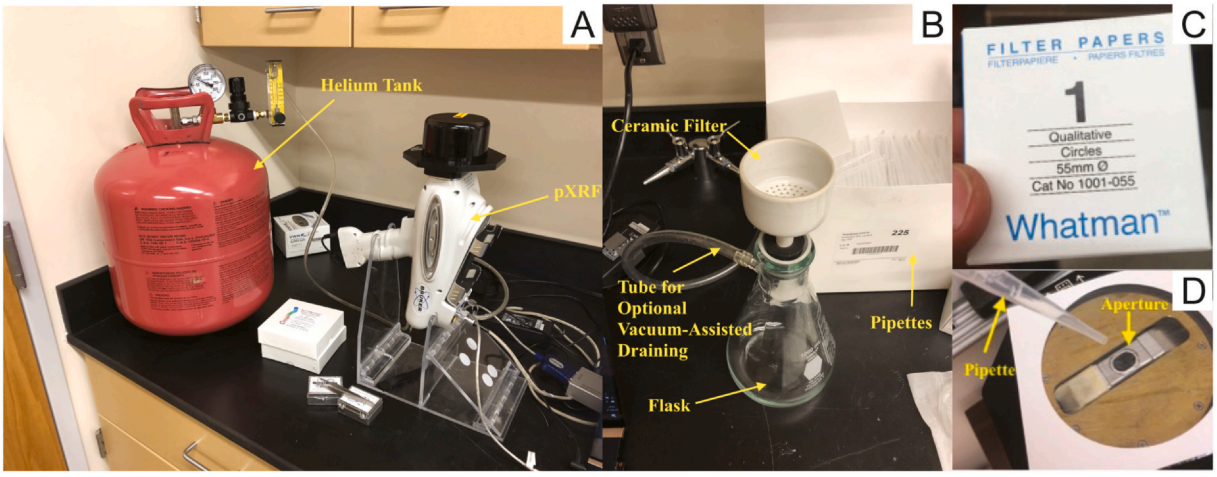

Fig. 2. A) The pXRF setup with in-line He gas displayed as used at the University of Utah during analysis. B) Setup for filtration of heated samples. C) Filter paper used for filtration. D) Application of 0.5 mL aliquot on to thin-film for analysis with pXRF.

Table 2
Corrections factors and spectral normalization ranges used for building inter-elemental calibration models in S1 CalProcesses.

Prediction	Corrections												Normalization range (keV)
Ions	Na Kα		Mg Kα		S Kα		Cl Kα		K Kα		Ca Kα		
	S	BG	S	BG	S	BG	S	BG	S	BG	S	BG	
Na^+	x	x					x	x					1.9–2.1
Mg^{2+}		x		x			x	x					1.9–2.1
SO_4^{2-}					x	x	x	x					1.9–2.1
Cl^-							x	x					4.2–4.4
K^+								x		x	x	x	4.2–4.4
Ca^{2+}									x	x	x	x	4.2–4.4

S = slope correction.
BG = background correction.

spectra at any energy non-linearly correlates to concentrations of elements in an analyzed sample with known characteristic fluorescence at that energy, not counting for spectral artifacts of the detector (e.g. Si escape peak, sum peaks, etc.)

The spectral response for these samples show dominant spectral features consistent with high chloride concentrations (Fig. 3). For calibration, separate normalization energy ranges within the spectra were used for the two calibration models. The intensity of the Cl Kα fluorescence peak (2.62 kiloelectron Volts (keV)) defines the background spectral intensities across energy ranges from 1.04–2.31 keV associated with the fluorescence peaks for the lightest elements quantifiable by this pXRF method (Na—S). As such, two samples with the same concentration of Mg^{2+}, but different Cl^- concentrations can exhibit very different background spectral intensities from 1.04–2.31 keV, and therefore different Mg Kα (1.25 keV) spectral peak intensities. The effect of Cl^- ion concentrations in solution on measurements of the ions with fluorescence at lower energies (Na^+–SO_4^{2-}) creates a need to calibrate separately for this range in the X-ray spectrum. Using 1.9–2.1 keV for spectral normalization (normalization window 1) corrects to this background intensity shift caused by Cl^-. Samples used for this study all have low concentrations of dissolved PO_4^{3-}, but this methodology directly overlaps with the P Kα fluorescence peak (2.01 keV). A different normalization window would need to be selected when using this method of calibration for waters with higher concentrations of dissolved P species. Using 4.2–4.4 keV for a spectral normalization (normalization window 2) in the range of Compton scattering, photon scattering of the X-ray source by the sample, was effective in calibrating for quantification of Cl^-, K^+, and Ca^{2+}.

3.2. Validated pXRF major ion concentrations

Comparison of pXRF results (i.e. inter-elemental calibrated major ion concentrations) to external lab results (i.e. external laboratory reference concentrations) for 12 validation samples showed highly correlated ($R^2 > 0.90$) results for five of the six major ions (Fig. 4). Calibrated pXRF concentrations for SO_4^{2-}, K^+, and Ca^{2+} were the most highly correlated results ($R^2 > 0.95$). Calibrated pXRF Na^+, Mg^{2+}, and Cl^- concentrations had lower correlations when compared to concentrations from external laboratory analyses.

The inter-elemental calibrated pXRF results for Na^+ were limited by both the relatively low intensity of Na Kα fluorescence peaks (1.04 keV) and the presence of large Cl—Si escape peaks (0.88 keV) reducing the reliability of Na Kα intensity to be used for accurate prediction of Na^+ concentrations. High photon flux from sample Cl^- concentrations resulted in the presence of a Cl—Si escape peak. This secondary Cl peak, shifted 1.74 keV down from the Cl Kα fluorescence peak (2.62 keV), was the result of the pXRF instrument's Si(Li) detector and the high flux of photons from Cl^- concentrations in samples. The Cl—Si escape peak had a photon intensity 10^2–10^3 greater in magnitude to the adjacent Na Kα fluorescence peak. This Cl—Si escape peak heavily masks detected photon responses to a wide range of Na^+ concentrations in solution.

Comparisons between pXRF and external laboratory results for the other 5 major ions yielded $R^2 > 0.90$. The largest inconsistency occurred with the validation of Mg^{2+} and Cl^- concentrations for a single Dead Sea brine. The Dead Sea has anomalously high Ca^{2+} concentrations relative to other cations (e.g. Na^+, Mg^{2+}) compared with most of the other Cl^- brines in this sample set. A shift in the relative cation and anion concentrations in dense brines likely constitutes a significant shift

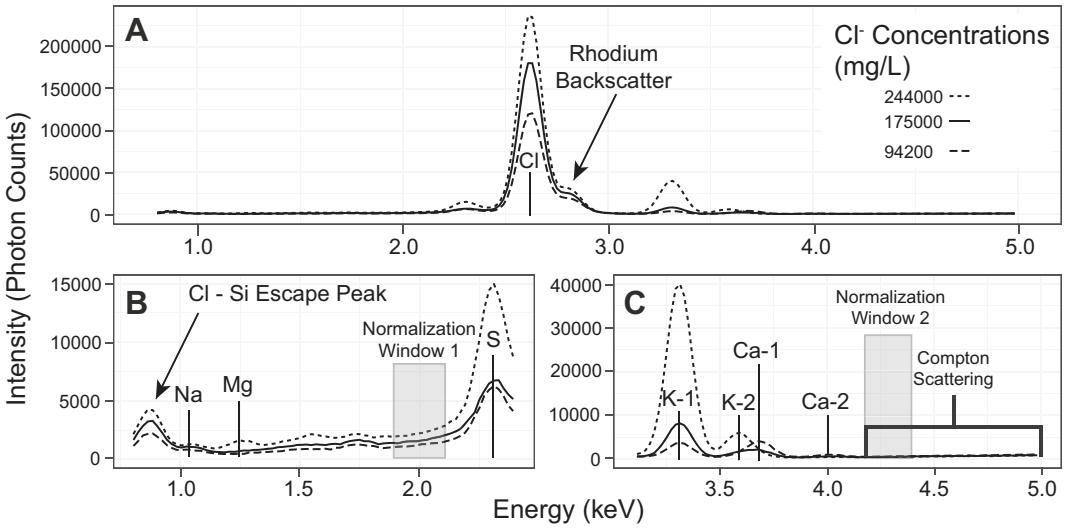

Fig. 3. Three example spectra with different line symbology (i.e. dotted, solid, dashed) from pXRF scans of samples with different chloride concentrations. A) The spectra from 0.5–5.0 keV shows a large Cl Kα peak (2.62 keV) with a rhodium backscatter "shoulder" from the X-ray source. B) The same spectra from 0.8–2.5 keV shows the photon response for elements Na—S. The baseline intensity is shifted for each spectrum and the normalization range (1.9–2.1 keV) used to correct in this part of the spectra is shown by the grey box (normalization window 1). A large Cl—Si escape peak (0.88 keV) is an effect from high Cl^- concentrations and the silicon detector of the instrument. C) These spectra plotted from 3.2–5.0 keV show the elemental photon response for K^+ and Ca^{2+} dissolved in solution and normalization range 2 (4.2–4.4 keV) used for prediction of Cl^-–Ca^{2+}.

in sample matrix. It is likely that a large shift in the brine matrix was responsible for inconsistency in calibrated results for this single sample as is common with other materials (e.g. rocks, sediments).

3.3. Instrument sensitivity to dissolved ion concentrations

Sample dilution results demonstrate different sensitivity to concentrations for each major ion (Fig. 5). Segmented linear regression models were used to determine inflection points in the comparison of pXRF measured photon counts and gravimetrically calculated diluted ion concentrations. Inflection points were interpreted as the concentration at which the photon response in no longer consistently sensitive to the concentration of an ion in solution. Photon responses show sensitivity to Mg^{2+} and Cl^- concentrations as low as 10^3 mg/L. Photon counts show consistent response for SO_4^{2+}, K^+, and Ca^{2+} concentrations from 10^0 to 10^2 mg/L. For SO_4^{2+} concentrations, there is a wide amount of variation in photon response, especially from 10^1 to 10^2 mg/L. One possible explanation for this is the assumption that

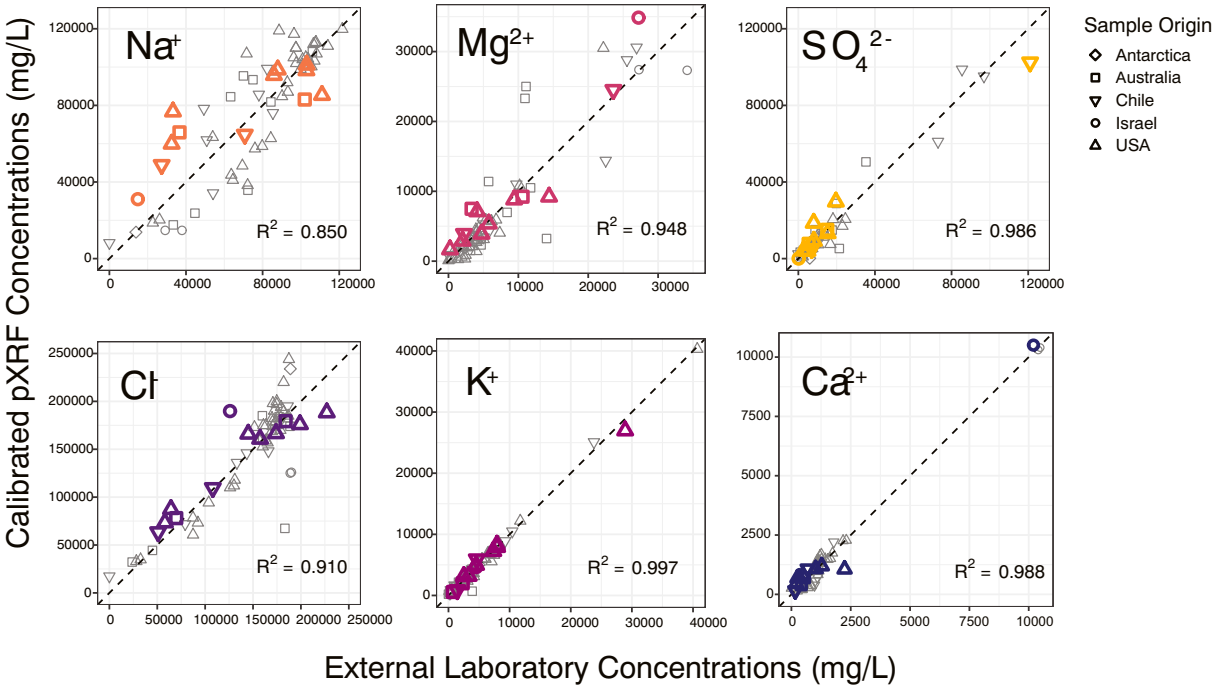

Fig. 4. External laboratory reference brine concentrations (mg/L) vs. pXRF inter-elemental calibrated concentrations (mg/L) for six major ions used for validation of this pXRF method (n = 12, bold and colored symbols) and reference samples used for the building of the inter-elemental calibrations (n = 52, grey symbols). Coefficients of determination (R^2) values label the fit of the inter-elemental calibration to laboratory reference concentrations for each major ion. Dashed lines represent a 1:1 relationship. Point shapes are consistent with Fig. 1 and validation sample point colors differentiate ions.

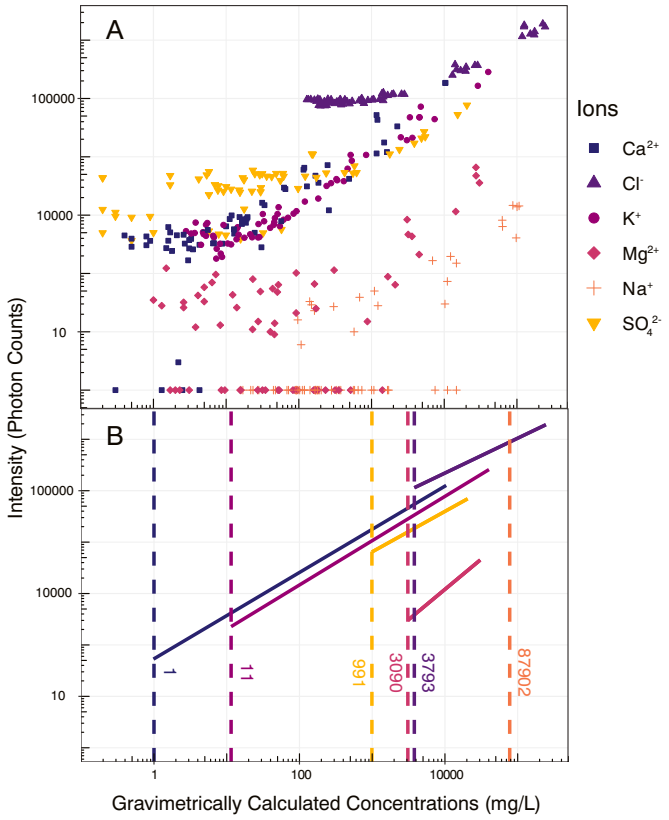

Fig. 5. A log-log plot of deconvoluted photon counts vs. gravimetrically calculated ion concentrations (mg/L) from original external laboratory reference values. A) All point values are plotted for each dilution of the subset samples (n = 64, 8 dilutions factors of 8 samples) for six major ions where each major ion is represented by unique color and shape. B) The model outputs of the first segment of each segmented linear model are shown (solid lines) and intersect the estimated breakpoints (dashed lines, colored text) in the model, interpreted as the lower detection limit for each ion. Colors are consistent with Fig. 4.

photon counts for the S Kα fluorescence peak correspond with SO_4^{2-} where other sulfur species may be present. These results indicate lower limit sensitivities of concentrations reliably detected in brine samples rather than precision. Precision for pXRF measurements will vary based on the matrix of samples being analyzed and the calibration used to produce quantified concentrations. The reliable photon responses for SO_4^{2-}, K^+, and Ca^{2+} are of particular interest in brines where saturation of gypsum and other sulfate minerals are under investigation. This includes many brines within the Atacama Desert where $MgSO_4$ precipitation interferes with solution mining of Li^+.

3.4. Brine Trace Element Content with pXRF

Analysis of brines samples shows exploring trace element content promising where concentrations approach that of some major ions (Fig. 6). Trace element content in brine samples was explored using samples (n = 57) where scans were made using both lower energy settings with helium and no filter as well as higher energy settings with the yellow filter (Al, Ti) and no helium. Sufficient ranges in trace element concentrations from external laboratory reference values were available to semi-quantitatively explore Al, Mn, Br, and Sr (n = 14, 16, 18, 36 respectively). Similar to major ions, pXRF sensitivity is limited to higher concentrations of 10^2–10^3 mg/L for lighter elements (e.g. Al, Mn). For higher atomic number elements (e.g. Br, Sr) relationships between photon intensity and concentration emerge in the range of 10^0–10^2 mg/L. Past work has estimated detection limits down to 3 ppm for $AgNO_3$ in dietary supplements, 21 ppm for Cu in water, and 28 ppm for Pb in water (Sánchez-Pomales et al., 2013; Zhou et al., 2018). Geochemical data available for the samples in this study were not robust enough to explore trace element concentrations in the same way as major ion results. However, these results do show the potential for future work on quantifying trace element concentrations in brines.

3.5. Areas for future investigation

Further experimentation of pXRF brine analysis could lead to better understanding of methodological possibilities, limitations, and the configuration of instrumentation optimization for brine geochemical analyses. Photon response from brines is different than with rock or sediment samples, and may require different energy and filter settings for optimization (Watts et al., 2018). Testing the response of pXRF to larger volumes than the 0.5 mL aliquot used in this study may allow greater excitation and thus, may yield improved analytical sensitivity (Zhou et al., 2018).

The calibration of analytical results for pXRF offers many choices that range across statistical models of photon data, semi-empirical methods using reference samples, and fundamental principles of X-ray physics. A wide variety of methods exist for the calibration of X-ray spectra with merits and limits for each (Steiner et al., 2017). While a proprietary software was applied for building the calibration for the results in this study, there are other options available. CloudCal is one available open-source software tool and graphical user interface for calibrations programmed in the R language and includes statistical predictions incorporating slope and peak interference as well as machine learning methods for the interpretation of X-ray spectra (Drake, 2018). Comparative tests of brines with pXRF using multiple calibration methods could optimize the proposed methodology in this study.

For pXRF matrix-specific calibration, concentrations in reference materials should cover a range of concentrations to include those for the quantification of unknown samples. This is equally true for brine samples, where ≥10% of a sample are dissolved solids that can vary in concentration of various cations and anions. For this study, most samples are concentrated chloride brines with variable relative cation concentrations. For better calibration to samples for a specific location or to brines with greater concentrations of other anions (e.g. SO_4^{2-}, HCO_3^-) calibration to those specific matrices are likely required. Clear fluorescence peaks were present for a number of trace elements (e.g. Al, Mn, Br, Sr) in this sample set and with the appropriate analytical data may be calibrated and quantified. This is particularly important in the analysis of acid brines, where these elements are major constituents (Bowen and Benison, 2009). Experimentation into brines with more variable cation and anion chemistry than presented in this study would be a valuable addition to the literature.

4. Conclusions

The application of pXRF to the analysis of major ion geochemistry in brines provides a method with minimal sample preparation. This approach is field portable, fast, non-destructive, and relatively inexpensive when compared with other analytical instrumentation. While this research demonstrates the effectiveness of pXRF to brines in a laboratory setting this can be translated to field studies. With steps taken to calibrate instrumentation prior to mobilization with appropriate reference materials this method is ready for portable applications in field settings.

Limitations of the presented methodology include the requirements of calibrating to a specific matrix and relatively low sensitivity to some ion concentrations. The demonstrated calibration methodology in this study performed well for the majority of Cl^- anion-dominate brines with the best correlation to external laboratory concentrations being for K^+ (R^2 = 0.997) and sensitivity in photon response reaching down to 11.2 mg/L. The largest discrepancy between pXRF and external laboratory concentrations were for Na^+ (R^2 = 0.850) with sensitivity in

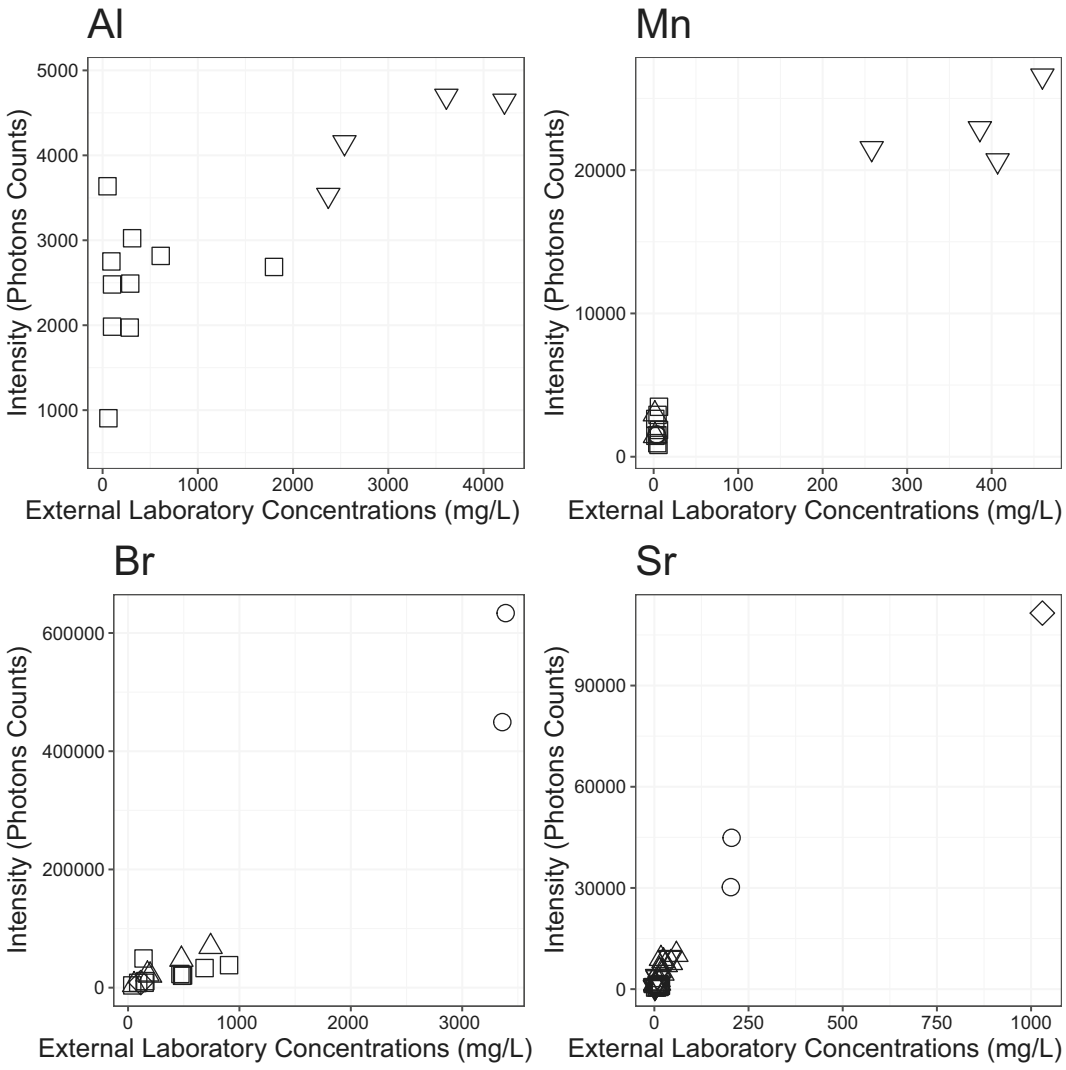

Fig. 6. Plots for four trace elements (Al, Mn, Br, Sr) in solution compare deconvoluted photon intensities to external laboratory concentrations. Symbology is the same as Figs. 1 and 4.

photon response reaching the upper limit of those samples tested in the dilution experiment.

The implementation of XRF for field studies in earth and planetary science is of relevance currently as the launch of the Mars 2020 rover (i.e. “Perseverance”) possesses a custom microXRF instrument onboard to perform the elemental analysis of Martian rocks and sediments on the surface and in the near surface to determine the depositional processes of these sediments and their relevance to the discovery of life on other planets (Allwood et al., 2015). Expanding the application of XRF to include brines is timely given that saline deposits both on Earth and Mars are targets for the preservation of ancient microbial life.

Declaration of competing interest

The authors declare that they have no known competing financial interests or personal relationships that could have appeared to influence the work reported in this paper.

Acknowledgments

Support for this research was provided by National Science Foundation – Dynamics of Coupled Natural and Human Systems Grant [#1617473] a University of Utah Global Change and Sustainability Center Graduate Research Grant, and the USGS Mineral Resources Program, Lithium Source to Sink project. Thank you to Dr. Nadav Lensky (Israeli Geological Survey), Craig Peterson (Intrepid Potash), as well as Roxanne Tea and Stephen Allen (U.S. Bureau of Land Management) for assistance with acquiring samples. Thank you to Dr. B. Lee Drake and Dr. Bruce Kaiser for discussions on the application and calibration of pXRF to brines. Thank you to Jory Lerback, Jeremiah Bernau, David O'Leary, and Krishangi Groover for their support and comments on this manuscript.

Data used for this work has been submitted to the Mendeley Data repository.

References

Allwood, A., Clark, B., Flannery, D., Hurowitz, J., Wade, L., Elam, T., Foote, M., Knowles, E., 2015. Texture-specific elemental analysis of rocks and soils with PIXL: the planetary instrument for X-ray lithochemistry on Mars 2020. In: IEEE Aerosp. Conf. Proc. 2015-June, 1–13.

Benison, K.C., 2019. The physical and chemical sedimentology of two high-altitude acid slars in Chile: Sedimentary processes in an extreme environment. J. Sediment. Res. 89, 147–167.

Benison, K.C., Bowen, B.B., 2015. The evolution of end-member continental waters: the origin of acidity in southern Western Australia. GSA Today 25, 4–10.

Benison, K.C., Karmanocky III, F.J., 2014. Could microorganisms be preserved in Mars gypsum? Insights from terrestrial examples. Geology 42, 615–617.

Bowen, B.B., Benison, K.C., 2009. Geochemical characteristics of naturally acid and

alkaline saline lakes in southern Western Australia. Appl. Geochem. 24, 268–284.
Bowen, B.B., Benison, K.C., Story, S., 2012. Early diagenesis by modern acid brines in Western Australia and implications for the history of sedimentary modification on Mars importance of Western Australia acid brine environments. SEPM J. Sediment. Res. 229–252.
Brewer, P.G., Spencer, D.W., 1969. A note on the chemical composition of the Red Sea brines. In: Hot Brines and Recent Heavy Metal Deposits in the Red Sea.
Carpenter, A.B., 1978. Origin and chemical evolution of brines in sedimentary basins. SPE Annu. Fall Tech. Conf. Exhib.
Dickson, J.L., Head, J.W., Levy, J.S., Marchant, D.R., 2013. Don Juan Pond, Antarctica: Near-surface CaCl 2-brine feeding Earth's most saline lake and implications for Mars. Sci. Rep. 3, 1–8.
Drake, B.L., 2018. CloudCal.
Hardie, L.A., Eugster, H.P., 1970. The Evolution of Closed-Basin Brines. Miner. Soc. Amer. Spec. Pap. 3, 273–290.
Hunt, A.M.W., Speakman, R.J., 2015. Portable XRF analysis of archaeological sediments and ceramics. J. Archaeol. Sci. 53, 628–638.
Kipnis, E.L., Bowen, B.B., 2018. Observations of salt crust change from 1960–2016 and the role of humans as geologic agents at the Bonneville Salt Flats, Utah. In: Geofluids of Utah, pp. 287–303.
Melquiades, F.L., Parreira, P.S., Appoloni, C.R., Silva, W.D., Lopes, F., 2011. Quantification of metals in river water using a portable EDXRF system. Appl. Radiat. Isot. 69, 327–333.
Muggeo, V.M.R., 2003. Estimating regression models with unknown break-points. Stat. Med. 22 (19), 3055–3071.
Muggeo, V.M.R., 2008. Segmented: an R package to fit regression models with broken-line relationships. In: R News. 8. R Project, pp. 20–25.
Muggeo, V.M.R., 2016. Testing with a nuisance parameter present only under the alternative: a score-based approach with application to segmented modelling. J. Stat. Comput. Simul. 86, 3059–3067.
Muggeo, V.M.R., 2017. Interval estimation for the breakpoint in segmented regression: a smoothed score-based approach. Aust. New Zeal. J. Stat. 59 (3), 311–322.
Munk, L.A., Hynek, S.A., Bradley, D., Boutt, D.F., Labay, K., Jochens, H., 2016. Lithium brines: a global perspective. Rev. Econ. Geol. 18, 339–365.
Ojha, L., Wilhelm, M.B., Murchie, S.L., Mcewen, A.S., Wray, J.J., Hanley, J., Massé, M., Chojnacki, M., 2015. Spectral evidence for hydrated salts in recurring slope lineae on Mars. Nat. Geosci. 8 (11), 829–832.
Pearson, D., Chakraborty, S., Duda, B., Li, B., Weindorf, D.C., Deb, S., Brevik, E., Ray, D.P., 2017. Water analysis via portable X-ray fluorescence spectrometry. J. Hydrol. 544, 172–179.
Rowe, H., Hughes, N., Robinson, K., 2012. The quantification and application of handheld energy-dispersive x-ray fluorescence (ED-XRF) in mudrock chemostratigraphy and geochemistry. Chem. Geol. 324–325, 122–131.
Sánchez-Pomales, G., Mudalige, T.K., Lim, J.H., Linder, S.W., 2013. Rapid determination of silver in nanobased liquid dietary supplements using a portable X-ray fluorescence analyzer. J. Agric. Food Chem. 61, 7250–7257.
Sirota, I., Enzel, Y., Lensky, N.G., 2017. Temperature seasonality control on modern halite layers in the Dead Sea: in situ observations. Bull. Geol. Soc. Am. 129, 1181–1194.
Steiner, A.E., Conrey, R.M., Wolff, J.A., 2017. PXRF calibrations for volcanic rocks and the application of in-field analysis to the geosciences. Chem. Geol. 453, 35–54.
Trumbo, S.K., Brown, M.E., Hand, K.P., 2019. Sodium chloride on the surface of Europa. Sci. Adv. 5 (6), 1–4.
Warren, J.K., 1996. Evaporites, brines and base metals: what is an evaporite? Defining the rock matrix. Aust. J. Earth Sci. 43, 115–132.
Watts, J.C., King, J.L., Dyar, M.D., Ytsma, C., Bleacher, J., McAdam, A., Hurowitz, J., Young, K., 2018. Filter selection for analysis of geological samples with handheld bruker tracer xrf. In: 49th Lunar and Planetary Science Conference 2018.
Welch, K.A., Lyons, W.B., Graham, E., Neumann, K., Thomas, J.M., Mikesell, D., 1996. Determination of major element chemistry in terrestrial waters from Antarctica by ion chromatography. J. Chromatogr. A 739, 257–263.
Zhou, S., Yuan, Z., Cheng, Q., Zhang, Z., Yang, J., 2018. Rapid in situ determination of heavy metal concentrations in polluted water via portable XRF: using Cu and Pb as example. Environ. Pollut. 243, 1325–1333.